Nonprehensile Object Transportation with a Legged Manipulator

Viviana Morlando, Mario Selvaggio, Fabio Ruggiero

Abstract— This paper tackles the problem of nonprehensile object transportation through a legged manipulator. A whole-body control architecture is devised to prevent sliding of the object placed on the tray at the manipulator's end-effector and retain the legged robot balance during walking. The controller solves a quadratic optimization problem to realize the sought transportation task while maintaining the contact forces between the tray and the object and between the legs and the ground within their respective friction cones, also considering limits on the input torques. An extensive simulation campaign confirmed the feasibility of the approach and evaluated the control performance through a thorough statistical analysis conducted varying mass, friction, and the dimension of the transported object.

I. INTRODUCTION

Service robots are developed to assist humans during dull, dangerous, or repetitive tasks. To date, several service robots have been developed and deployed in different fields ranging from tourism and hospitality [1], [2] to home care assistance [3], some of them being already a consumer product for domestic environments [4], [5]. To realize robots able to fulfill all these applications, the research in service robotics has been directed towards mobile manipulators that can traverse large spaces and execute manipulation tasks.

Most mobile robots developed in the last years are wheeled robots endowed with one or two arms [6]. Different mobile robots were designed to realize similar objectives by endowing them with the capabilities of executing complex manipulation tasks such as opening a door or picking items [7]. However, wheeled robots often encounter difficulties in unstructured environments with non-flat grounds, while legged robots can overcome these obstacles by effectively sensing and adapting their steps to the ground. This crucial ability enabled their wide employment in search and rescue scenarios in the most impervious sites where wheeled robots could remain stuck. Nevertheless, although their performance can exceed those of wheeled robots in certain situations, legged robots still need to find their space in the service fields of household or hospitality.

In the past, biped robots have been used for elderly care assistance [3], [8]. However, robots with more legs (e.g., quadrupeds, hexapods, etc.) inherently possess greater stability ranges and higher mobility degrees [9]. To widen their spectrum of applications, the recent trend is to endow
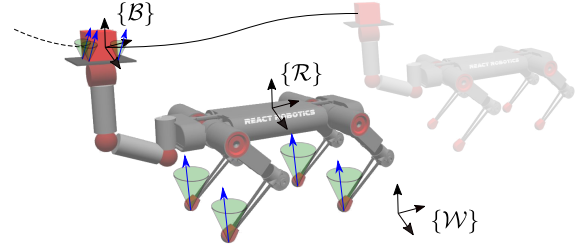
Fig. 1. A legged manipulator has to transport an object (red cube) placed on a tray-like end-effector along a trajectory (black) from a starting configuration (transparent) while simultaneously preventing its sliding by keeping contact forces (blue) inside the friction cones (green).

multi-legged robots with arms that make them capable of grasping and manipulating objects [10] enabling interaction-based tasks such as opening a hinged door [11].

Despite their unique features, legged robots have rarely shown nonprehensile manipulation skills so far and usually employ their legs to perform these actions [12], [13]. Nonprehensile manipulation can be considered one of the most complex task [14] since it is neither possible to prevent infinitesimal motions of the object nor to resist all the external wrenches applied to it. However, endowing legged robots with this capability would enable them to perform a broader range of dexterous manipulation tasks, which are critical in the field of service robotics.

This paper tackles the problem of transporting an object from an initial to the goal pose without firmly grasping it using a legged manipulator. Carrying a payload modifies the robot's dynamics, which must not only counteract but also regulate its motion to satisfy non-sliding constraints for both locomotion and manipulation tasks jointly. Differently from [15], these constraints are addressed in a unified and principled way through an optimization-based whole-body controller for a legged robot transporting an object on a tray in a nonprehensile configuration, which is the main contribution of this work. To the authors' knowledge, this is the first work in which a legged manipulator is used for nonprehensile transportation tasks. The performance of the legged loco-manipulation system is statistically evaluated in a simulation campaign considering different mass, friction, and dimensions of the object.

II. RELATED WORKS

Over the years, many different control methods were realized to achieve dynamic locomotion, especially for quadruped robots, since they possess a higher stability range than biped robots, and their legs are more manageable to coordinate than robots with six or more legs. Some approaches used a reduced dynamic model [16], limiting the dynamicity

of the robot. Controllers based on whole-body dynamics need to be adopted to avoid this situation, allowing allows the decoupling of the motion planning from the control problem as shown in [17]. This control approach was modified in [18], [19] to modulate the ground reaction forces. Whenever a legged robot is endowed with a robotic arm, the system dynamics change, and the controller needs to account for both locomotion and manipulation tasks. In [20], tracking of the desired trajectory for the base was handled separately from the one related to the arm. However, the framework was not tested for a manipulation task: it just demonstrated the controller's capability to guarantee a stable walk. Differently, two whole-body controllers were realized to handle loco-motion and manipulation tasks altogether in [10], [11]. The approaches showed robustness during different manipulation tasks, such as pushing and opening a door. This enabled haptic teleoperation of a legged manipulator [21], where the teleoperation managed the arm during stance mode and the robot's base during the locomotion.

However, none of the above works considered a legged robot transporting an object in a nonprehensile way. For instance, the contact forces computed by the planner in [11] are directly used as references in the robot whole-body control. Since there is no knowledge of the object's dynamics inside this last, it would not be possible to define a prioritized task on the object's motion level. This aspect is crucial to avoid sliding during transportation, making it impossible to handle the addressed problem with the work above. Indeed, when the robot does not firmly grasp an object, there exist motions induced by inertial or external forces that can not always be inhibited [22]. In such a case, the object can still be manipulated, typically realizing a sequence of opportunely combined nonprehensile manipulation primitives [14], [23]. These include throwing [24], catching [25], batting [26], pushing [27], rolling [28], and so on.

We restrict our related works' overview to the so-called dynamic grasping (or nonsliding) manipulation primitive, which immobilizes the object to the robot palm (as it was firmly grasped) by exploiting gravity, inertial, and frictional forces. The nonsliding manipulation primitive was employed in [8], where a waiter humanoid robot transporting objects on a tray is developed. A motion planning framework that explicitly considers reaction and friction forces as kino-dynamic constraints for the nonprehensile transportation of a bottle was proposed in [29]. A task priority control scheme, featuring sliding mode and admittance control, for human-robot collaborative transportation of an object on a tray, was designed in [30]. On the same line, teleoperation architec-tures were designed to safely transport an object placed on a tray [15]. However, despite the significant amount of work in the field, nonprehensile object transportation via dynamic grasping has never been shown on a quadruped robot.

III. SYSTEM MODEL

A. Transported object

The object dynamics must be taken into account to deal with the transportation problem. Consider an object trans-ported by a tray-like end-effector mounted onto a robotic platform. The following assumptions are introduced [15]: A1) the object dynamic properties and shape are known and considered to be those of a rectangular cuboid; A2) the initial object's pose relative to the tray is known; A3) the tray/object interaction is modeled through a finite set of contact points located on the object vertexes facing the tray; A4) the set of wrenches that are transmitted across the contacts is constituted only by linear forces (point contacts with friction model [31]); A5) the object/tray Coulomb friction coefficient is uniform and known. Let $q_b = (p_b, R_b) \in SE(3)$ be the pose of the object frame $\{\mathcal{B}\}$ (Fig. 1) attached to the object's center of mass (CoM), in the inertial reference frame $\{\mathcal{W}\}$, with $p_b \in \mathbb{R}^3$ the position vector of the object and $R_b \in SO(3)$ the orientation of $\{\mathcal{B}\}$ in $\{\mathcal{W}\}$. The object dynamics can be written as

$$M_b \dot{\mathcal{V}}_b + C_b(\mathcal{V}_b)\mathcal{V}_b + N_b(R_b) = \mathcal{F}_b, \tag{1}$$

with $M_b \in \mathbb{R}^{6 \times 6}$ the constant and positive-definite object's mass matrix, constructed from the object's mass $m \in \mathbb{R}_{\geq 0}$ and the constant symmetric and positive-definite inertia matrix $I_b \in \mathbb{R}^{3 \times 3}$; $C_b \in \mathbb{R}^{6 \times 6}$ the matrix accounting centrifugal/Coriolis effect; $N_b(R_b) \in \mathbb{R}^6$ the vector contain-ing gravity terms; $\mathcal{V}_b = (v_b, \omega_b) \in \mathbb{R}^6$ the body object's twist with $v_b \in \mathbb{R}^3$ the linear velocity and $\omega_b \in \mathbb{R}^3$ the angular velocity; $\mathcal{F}_b \in \mathbb{R}^6$ is the wrench exerted at the object's center of mass, expressed in $\{\mathcal{B}\}$. The body wrench $\mathcal{F}_b$ is dictated by the tray/object contact forces. Given the assumptions A1–A3, the number of contact points is $n_c = 4$, corresponding to the vertexes of the cube facing the tray. A suitable contact model is adopted to control the tray/object interaction behaviour [15]. Through A4, consider the stacked vector $F_c = \left[f_{c_1}^{\mathrm{T}}, ..., f_{c_{n_c}}^{\mathrm{T}} \right]^{\mathrm{T}} \in \mathbb{R}^{3n_c}$, containing the linear contact forces $f_{c_i} \in \mathbb{R}^3$ at the i-th contact point. The vector F_c is mapped to $\mathcal{F}_b$ through the grasp matrix $G \in \mathbb{R}^{6 \times 3n_c}$

$$\mathcal{F}_b = GF_c, \quad G = \left[Ad_{q_{b,c_1}^{-1}}^{\mathrm{T}} B_{c,1}, ..., Ad_{q_{b,c_{n_c}}^{-1}}^{\mathrm{T}} B_{c,n_c} \right], \tag{2}$$

where $Ad_{q_{b,c_i}^{-1}}^{\mathrm{T}} = \begin{bmatrix} R_{b,c_i}^b & O_{3 \times 3} \\ \hat{p}_{b,c_i}^b R_{c_i,b}^b & R_{b,c_i}^b \end{bmatrix}$, $B_{c,i} = \begin{bmatrix} I_{3 \times 3} \\ O_{3 \times 3} \end{bmatrix}$, with $I_\times$ and $O_\times$ the identity and zero matrices, respectively, of proper dimensions; $\hat{p}_{b,c_i}^b \in so(3)$ the skew-symmetric ma-trix associated with the vector $p_{b,c_i}^b \in \mathbb{R}^3$, being the position of the i-th contact point; $R_{b,c_i}^b \in SO(3)$ the orientation of the frame $\{\mathcal{C}_i\}$ of the i-th contact, all specified with respect to $\{\mathcal{B}\}$. In order to obtain a safe object transportation, the contact model must be characterized by a nonsliding behaviour, meaning that each contact force vector $f_{c_i} \in \mathbb{R}^3$ must be contained inside the $i-$th friction cone FC_i. The $i-$th friction cone can be defined as the set of generalized contact forces realizable given the friction coefficient μ, between the object and the tray. Whenever $F_c \in FC = FC_1 \times \cdots \times FC_{n_c}$, the object can be manipulated without sliding with respect to the tray. This constraint can be expressed in linear form by approximating the i-th friction cone with a polyhedral cone generated by a finite set of unit vectors $\hat{f}_{c_i,j} \in \mathbb{R}^3$. The number of unit vectors $k \in \mathbb{N}_{>0}$ that

constitute the approximated friction cone's edges is free to be picked. To approximate the friction cone with an inscribed pyramid we considered $k = 4$ in this work [15]. However, a tighter approximation of the circular cone can be obtained by using more edges. The $j-$th edge can be calculated as $\hat{f}_{c_i,j} = R_z(2\pi j/k)R_y(\theta)\hat{z}, \quad \forall j \in \{1,\ldots,k\}$ where $\theta = \arctan\mu$, R_z and R_y are elementary rotation matrices. The constraint is formulated expressing f_{c_i} as a non-negative linear combination of unit vectors $\hat{f}_{c_i,1}\ldots\hat{f}_{c_i,k} \in \delta FC_i$, with δFC_i denoting the boundary of the i-th cone manifold, i.e., $FC_{c_i} = \left\{f_{c_i} \in \mathbb{R}^3 : f_{c_i} = \sum_{j=1}^k \lambda_{c_i,j}\hat{f}_{c_i,j}, \quad \lambda_{c_i,j} \geq 0\right\}.$

By denoting $\Lambda_b = \left[\lambda_{c_{1,1}}, \ldots, \lambda_{c_{n_c,k}}\right] \in \mathbb{R}^{kn_c}$ and $\hat{F}_c = \text{blockdiag}(\hat{F}_{c,1}, \ldots, \hat{F}_{c,n_c})$, with $\hat{F}_{c,i} = \left[\hat{f}_{c_i,1}, \ldots, \hat{f}_{c_i,k}\right]$, the stacked vector of contact forces can be compactly rewritten as $F_c = \hat{F}_c\Lambda_b$. When a non-sliding behaviour is desired it is sufficient to impose $\Lambda_b \geq 0$ to constrain all the contact forces inside the respective cones. This approach has demonstrated good performance with real hardware [15].

B. Legged robot manipulator

A legged robot endowed with a robotic arm can be described as a free-floating base with the legs and the arm attached. The free-floating base is usually modelled through six virtual joints giving six degrees of freedom (DoFs) in $\{\mathcal{W}\}$. The floating base position can be described by an arbitrary fixed point on the main body. Nevertheless, since the position of the robot's CoM is crucial for balancing, the dynamic model of a legged robot can be formulated in terms of the global CoM through the transformation introduced in [32]. Let $q_r = (p_r, R_r) \in SE(3)$ be the pose of the frame $\{\mathcal{R}\}$ attached to the robot's CoM, with $p_r \in \mathbb{R}^3$ the position vector of the robot's CoM and $R_r \in SO(3)$ the orientation of the frame $\{\mathcal{R}\}$ in $\{\mathcal{W}\}$. Besides, let $\mathcal{V}_r = (v_r, \omega_r) \in \mathbb{R}^6$ the twist of the frame $\{\mathcal{R}\}$ with respect to $\{\mathcal{W}\}$, with $v_r \in \mathbb{R}^3$ the linear velocity and $\omega_r \in \mathbb{R}^3$ the angular velocity. Finally, let $q \in \mathbb{R}^n$ be the vector collecting the arm and legs' joints. With this transformation, the legged system dynamics equipped with an arm is

$$\begin{bmatrix} M_{com}(q) & O_{6\times n} \\ O_{n\times 6} & M_q(q) \end{bmatrix}\dot{v} + \begin{bmatrix} O_{6\times 6+n} \\ C_q(q,v) \end{bmatrix}v + \begin{bmatrix} m_r g \\ 0_n \end{bmatrix} = \begin{bmatrix} 0_6 \\ \tau \end{bmatrix} + \begin{bmatrix} J_{st,com}(q)^{\mathrm{T}} \\ J_{st,j}(q)^{\mathrm{T}} \end{bmatrix}F_{gr} + \begin{bmatrix} J_{com}(q)^{\mathrm{T}} \\ J_q(q)^{\mathrm{T}} \end{bmatrix}F_{ext} + \begin{bmatrix} J_{r,com}^b(q)^{\mathrm{T}} \\ J_{r,j}^b(q)^{\mathrm{T}} \end{bmatrix}F_c,$$

$$(3)$$

with n the number of actuated joints of the legs and the arm; $v = \begin{bmatrix} \mathcal{V}_r^{\mathrm{T}} & \dot{q}^{\mathrm{T}} \end{bmatrix}^{\mathrm{T}} \in \mathbb{R}^{6+n}$ the stacked velocity vector; $m_r \in \mathbb{R}_{>0}$ is the total mass of the robot; $F_{gr} = \left[f_{gr_1}^{\mathrm{T}}, \ldots, f_{gr_{n_{st}}}^{\mathrm{T}}\right]^{\mathrm{T}} \in \mathbb{R}^{3n_{st}}$ are the ground reaction forces, with $0 < n_{st} \leq n_l$ the number of stance legs and n_l the number of legs; $F_{ext} \in \mathbb{R}^{3n_l}$ the stacked vector containing the resultant force at the legs' tips accounting for unmodelled dynamics and disturbances at any point of the robot; $J_r^b(q) = \begin{bmatrix} J_{r,com}^b(q) & J_{r,j}^b(q) \end{bmatrix} \in \mathbb{R}^{3n_c\times(6+n)}$ the body Jacobian of the tray/object contact points [15]; while all the other matrices are the same ones defined in [33] maintaining the assumptions that the trunk's angular motion is slow and

that the legs' and arm's masses are negligible with respect to the robot's total mass.

The same contact model presented in III-A is used to represent the ground reaction forces as $F_{gr} = \hat{F}_{gr}\Lambda_{gr}$, with $\Lambda_{gr} = \left[\lambda_{gr_{1,1}}, \ldots, \lambda_{gr_{n_{st},k}}\right] \in \mathbb{R}^{kn_{st}}$ and $\hat{F}_{gr} = \text{blockdiag}(\hat{F}_{gr,1}, \ldots, \hat{F}_{gr,n_{st}})$, with $\hat{F}_{gr,i} = \left[\hat{f}_{gr_i,1}, \ldots, \hat{f}_{gr_i,k}\right]$, describing the friction cone manifold, considering μ_{gr} the friction coefficient of the floor. As for the object problem, to have a nonsliding behaviour of the feet and retain the balance, it must be $\Lambda_{gr} \geq 0$ to constrain the forces inside the cones.

IV. OPTIMIZATION-BASED CONTROLLER

A. Problem statement and architecture description

The addressed problem is to transport the object placed on a tray at the arm's end-effector to the desired pose $\hat{q}_{b,d} = (\hat{p}_{b,d}, \hat{R}_{b,d}) \in SE(3)$ following the desired trajectory. The control architecture must prevent the object from sliding on the tray and retain the robot's balance during the motion. A motion planner and an optimization problem shape the designed whole-body controller. The motion planner is thus separated from the control problem. The motion is continuously replanned based on the current robot's state, according to the desired trajectory. A foot scheduler is used to switch the stance and swing legs according to the desired gait [18]. Moreover, the momentum-based observer presented in [33] is included in the framework to robustify the control by rejecting external disturbances, it is not presented for brevity.

B. Motion planner

The motion planner computes the references for the object, the CoM, and the swing feet inside the quadratic problem. Considering the set-point, a desired trajectory $q_{b,ref} = (p_{b,ref}, R_{b,ref}) \in SE(3)$, $\mathcal{V}_{b,ref} = (\dot{p}_{b,ref}, \omega_{b,ref}) \in \mathbb{R}^6$ and $\dot{\mathcal{V}}_{b,ref} = (\ddot{p}_{b,ref}, \dot{\omega}_{b,ref}) \in \mathbb{R}^6$ for the object is computed as 3-rd order spline using a planner based on artificial potentials to avoid obstacles in the environment. Moreover, the condition $\dot{\mathcal{V}}_{b,ref,z} < g$ is imposed, so that the desired linear acceleration of the object along the z-axis of $\{\mathcal{W}\}$, aligned with the gravity vector, would never be greater than the gravity acceleration. Such situation can cause an instantaneous detachment between the object and the tray and must be avoided. Since the objective here is a pure object transportation, the movement of the floating base relatively to the arm is not relevant. For this reason, the desired trajectory for the CoM is computed from the object's one. Considering the initial pose of the frame $\{\mathcal{R}\}$ with respect to $\{\mathcal{B}\}$ as $\bar{q}_{b,r} = (\bar{p}_{b,r}, \bar{R}_{b,r}) \in SE(3)$, the desired trajectory of the CoM can be computed in any instant $t > 0$ as $q_{r,d}(t) = q_{b,ref}(t) +^* \bar{q}_{b,r}$, where the $+^*$ is defined as the addition operator for both the translational part and the orientation [34]. In this way, the configuration of the robot will be similar to the starting one in each instant. Notice that, in case of more complex tasks, separate reference inputs can be considered for the object and the CoM. The motion of the robot is then divided into footsteps, each of one is composed by a stance and a swing phases. A foot scheduler is used to

switch the stance and swing legs according to the desired gait. At the start of each footstep, the motion of the CoM is continously replanned following the desired trajectory $q_{r,d}$, so that the ZMP is always mantained inside the support polygon to retain the balance. For this reason, the references for the CoM $q_{r,ref} = (p_{r,ref}, R_{CoM,ref}) \in SE(3)$, $\mathcal{V}_{r,ref} = (\dot{p}_{r,ref}, \omega_{r,ref}) \in \mathbb{R}^6$ and $\dot{\mathcal{V}}_{r,ref} = (\ddot{p}_{r,ref}, \dot{\omega}_{r,ref}) \in \mathbb{R}^6$ are computed as a 3-rd order spline using the ZMP-criterion [33]. The reference $x_{sw,d} \in \mathbb{R}^{3(n_l - n_{st})}$ for the swing feet is computed using two splines: the former to lift the foot, the latter to lower it. Considering $T_{sw} > 0$ as the duration of the swing phase, each spline lasts for $0.5 T_{sw}$ [33].

C. Quadratic problem

The optimization problem proposed here employs centroidal and object dynamics to track the floating base and object motion references, respectively. The chosen vector of control variables is $\zeta = \begin{bmatrix} \dot{v}^{\mathrm{T}} & \Lambda_{gr}^{\mathrm{T}} & \Lambda_b^{\mathrm{T}} \end{bmatrix}^{\mathrm{T}} \in \mathbb{R}^{n_v}$, with $n_v = 6 + n + kn_{st} + kn_c$. The problem, further described in the following, has the following form

$$\underset{\zeta}{\text{minimize}} \quad f(\zeta) \qquad (4)$$

$$\text{subject to} \quad A\zeta = b, \qquad (5)$$

$$D\zeta \leq c. \qquad (6)$$

1) Cost Function $f(\zeta)$: The problem aims at tracking both the CoM's reference and the object's reference, minimising the control effort. Using the references from the motion planner, the desired wrench at the robot's CoM $\mathcal{F}_{com,ref}$ can be written using (3) as $\mathcal{F}_{com,ref} = K_{p,com}\mathcal{E}_r + K_{d,com}\dot{\mathcal{E}}_r + mg + M_{com}(q)\dot{\mathcal{V}}_{r,ref}$, with $K_{p,com}, K_{d,com} \in \mathbb{R}^{6 \times 6}$ positive definite matrices; $\mathcal{E}_r = \begin{bmatrix} e_{r,p}^{\mathrm{T}} & e_{r,o}^{\mathrm{T}} \end{bmatrix}^{\mathrm{T}} \in \mathbb{R}^6$ including both the position error $e_{r,p} = [p_{r,ref} - p_r] \in \mathbb{R}^3$ and the orientation error $e_{r,o} = \Delta\varphi_r \in \mathbb{R}^3$, both expressed in $\{\mathcal{W}\}$. The desired body wrench $\mathcal{F}_{b,ref}$ for the object can be computed using an inverse dynamics control law, derived from (1) as $\mathcal{F}_{b,ref} = M_b y + C_b(\mathcal{V}_b)\mathcal{V}_b + N_b(R_b)$, with $y = \dot{\mathcal{V}}_{b,ref} + K_{d,b}\dot{\mathcal{E}}_b + K_{p,b}\mathcal{E}_b$; $K_{p,b}, K_{d,b} \in \mathbb{R}^{6 \times 6}$ positive definite matrices; $\mathcal{E}_b = \begin{bmatrix} e_{b,p}^{\mathrm{T}} & e_{b,o}^{\mathrm{T}} \end{bmatrix}^{\mathrm{T}} \in \mathbb{R}^6$ including both the position error $e_{b,p} = R_b^{\mathrm{T}}[p_{b,ref} - p_b] \in \mathbb{R}^3$ and the orientation error $e_{b,o} = R_b^{\mathrm{T}}\Delta\varphi \in \mathbb{R}^3$ with $\Delta\varphi$ being the exponential coordinates of the rotation, i.e., $\Delta\varphi = \Delta\theta\hat{n}$, with $\hat{n}$ being the rotation axis and $\Delta\theta$ being the corresponding angle, both extracted from the rotation matrix $R_e = R_{b,ref}R_b^{\mathrm{T}}$ through the logarithmic map [31], both expressed in body frame. Considering $\hat{F}_{ext}$ the estimation of the momentum-based observer integrated in the framework, it can be split into $\hat{F}_{st} \in \mathbb{R}^{3n_{st}}$, the estimated forces regarding the support legs, and $\hat{F}_{sw} \in \mathbb{R}^{3(n_l - n_{st})}$, the estimated forces regarding the swing legs. The optimization can be defined as a multi-objective quadratic problem, with two objective functions aiming to track the desired wrench at the robot's CoM and the desired wrench at the object's CoM, respectively

$$f_1(\zeta) = \left\| J_{st,com}^{\mathrm{T}}\hat{F}_{gr}\Sigma_1\zeta + J_{st,com}^{\mathrm{T}}\hat{F}_{st} - \mathcal{F}_{com,ref} \right\|_{Q_1}, \qquad (7)$$

$$f_2(\zeta) = \left\| G\hat{F}_c\Sigma_2\zeta - \mathcal{F}_{b,ref} \right\|_{Q_2}, \qquad (8)$$

with $\| \cdot \|_{\times}$ the quadratic form with proper matrix; $\Sigma_1 \in \mathbb{R}^{kn_{st} \times n_v}$ and $\Sigma_2 \in \mathbb{R}^{kn_c \times n_v}$ two matrices selecting the elements of ζ representing the ground reaction and the object/tray contact forces, respectively ; $J_{st,com}^{\mathrm{T}}\hat{F}_{st}$ compensates for the stance legs' disturbance; $Q_1, Q_2 \in \mathbb{R}^{6 \times 6}$ symmetric and positive definite matrices used to specify the relative weight between the components of the cost function. Considering (7) and (8), a full cost function can be defined as

$$f(\zeta) = \left\| H\zeta - l \right\|_Q + \left\| \zeta \right\|_R, \text{ with } H = \begin{bmatrix} J_{st,com}^{\mathrm{T}}\hat{F}_{gr}\Sigma_1 \\ G\hat{F}_c\Sigma_2 \end{bmatrix} \in$$

$\mathbb{R}^{12 \times n_v}$ and $l = \begin{bmatrix} \mathcal{F}_{com,ref} - J_{st,com}^{\mathrm{T}}\hat{F}_{st} \\ \mathcal{F}_{b,ref} \end{bmatrix} \in \mathbb{R}^{12}$. The symmetric and positive definite matrices $Q \in \mathbb{R}^{12 \times 12}$ and $R \in \mathbb{R}^{n_v \times n_v}$ specify the relative weight between the cost function's components.

2) Equality constraints $A\zeta = b$: Three equality constraints need to be imposed. The first one constraints the control variable to be consistent with (3)

$$\begin{bmatrix} M_{com}(q) & O_{6 \times n} & -J_{st,com}(q)^{\mathrm{T}}\hat{F}_{gr} & -J_{r,com}^b(q)^{\mathrm{T}}\hat{F}_c \end{bmatrix}\zeta = $$
$$= -m_r g. \qquad (9)$$

The second equality constraint guarantees that the contact of the stance feet is maintained. This holds by imposing their velocity equal to zero as $J_{st}(q)v = 0_{3n_{st}}$, whose time derivative, in term of control variables, is

$$\begin{bmatrix} J_{st}(q) & O_{3n_{st} \times kn_{st}} & O_{kn_{st} \times kn_c} \end{bmatrix}\zeta = -\dot{J}_{st}(q, \dot{q})v. \qquad (10)$$

The third constraint imposes the velocity at the arm's end-effector in order to track the desired object motion

$$\begin{bmatrix} J_b^b(q) & O_{6 \times kn_{st}} & O_{6 \times kn_c} \end{bmatrix}\zeta = -\dot{J}_b^b(q)v + \dot{\mathcal{V}}_{b,ref} \qquad (11)$$

with J_b^b the object body Jacobian and $\dot{\mathcal{V}}_{b,ref}^b \in \mathbb{R}^6$ the desired object acceleration. Collecting (9), (10), and (11) yields defining the terms A and b in (5), omitted for brevity.

3) Inequality constraints $D\zeta \leq c$: Ground reaction forces and object/tray contact forces must be constrained to be inside the friction cones and guarantee the nonsliding behaviour

$$\Lambda_{c,i} \geq 0 \qquad \Lambda_{gr,i} \geq 0. \qquad (12)$$

Moreover, for mechanical and safety reasons, joint torques need always to be limited. Being $\tau_{min}, \tau_{max} \in \mathbb{R}^n$ the minimum and maximum reachable torques, respectively, considering the part of (3) regarding robot's actuated joints, the constraints about limited torques can be expressed as follows

$$\tau_{min} - C_q(q, v)\dot{q} \leq$$
$$\begin{bmatrix} O_{n \times 6} & M_q(q) & -J_{st,j}^{\mathrm{T}}(q)\hat{F}_{gr} - J_{r,j}^{b\mathrm{T}}(q)\hat{F}_c \end{bmatrix}\zeta \leq \qquad (13)$$
$$\tau_{max} - C_q(q, v)\dot{q}.$$

Finally, an equality constraint should be imposed to track the desired trajectory for the swing feet [33]: $\ddot{x}_{sw,cmd} = J_{sw}(q)\dot{v} + \dot{J}_{sw}(q, \dot{q})v$. where $\ddot{x}_{sw,cmd} = \ddot{x}_{sw,d} + K_{d,sw}(\dot{x}_{sw,d} - \dot{x}_{sw}) + K_{p,sw}(x_{sw,d} + -x_{sw}) - J_{sw}M_c^{-1}PJ_{sw}^T\hat{F}_{sw}$, with $J_{sw} \in \mathbb{R}^{3(n_l - n_{st}) \times 6 + n}$ the Jacobian whose transpose map the forces acting at the tip of
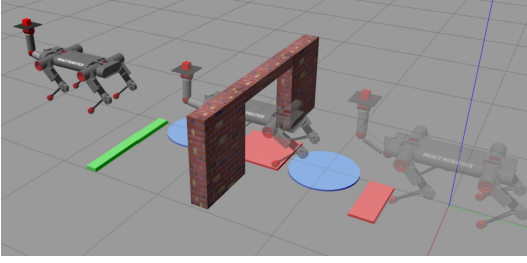
Fig. 2. Simulation setup and executed robot trajectory. Obstacles with different heights and friction coefficients are placed on the ground. A wall with a narrow gap is present along the robot desired path.

the swing legs into the acceleration of the CoM and the legs' joints; $P \in \mathbb{R}^{6+nn_l \times 6+nn_l}$ an orthogonal projection operator such that $PJ_{st}^{\mathrm{T}} = 0$, $P = P^2$, and $P = P^T$; $M_c = PM + I_{6+nn_l} - P$. This constraint is softened by adding slack variables $\gamma \in \mathbb{R}^{3(n_l - n_{st})}$ within the optimization problem. The addressed inequality constraint is chosen as [33]

$$\ddot{x}_{sw,cmd} - \gamma \le J_{sw}(q)\dot{v} + \dot{J}_{sw}(q,\dot{q})v \le \ddot{x}_{sw,cmd} + \gamma. \tag{14}$$

Therefore, collecting (12), (13), and (14), the terms c and D in (6) are retrieved, but they are here omitted for brevity.

4) Control torque: Given the result of the optimization problem, the control torques can be computed using the (3) as $\tau = M_q(q)\ddot{q} + C_q(q,v)\dot{q} - J_{st,j}(q)^T \hat{F}_{gr}\Lambda_{gr} - J_{r,j}^b(q)^{\mathrm{T}}\hat{F}_c\Lambda_b$, considering that all the external forces have been compensated for in the quadratic problem.

V. SIMULATION RESULTS

An extensive simulation campaign is carried out to validate the devised architecture. The analysis of the framework performance, taking into account the variability of the object's parameters is carried out. To this end, the object's mass m values $(0.2, 0.3, 0.4)$, the tray friction coefficient μ values $(0.4, 0.7, 1)$, and the object's side dimension d values $(0.06, 0.08, 0.1)$ are chosen.

A. Simulation setup

Simulations have been carried out with the Gazebo dynamic simulator (integrated in ROS). The addressed legged system is the DogBot from React Robotics, a quadruped (i.e., $n_l = 4$) open-source platform (see [33] for more details). The quadruped has been endowed with a 6-DoF arm (Fig. 1) inspired by the structure of the HyQ's centaur-like version [20], [35]. The realized arm has an overall weight of 4 kg. All the simulations were performed on a standard personal computer and are running in real-time.

The scenario used for testing our framework is shown in Fig. 2. A wall with a narrow gap, whose width and height are 1 m and 0.65 m, respectively, is positioned inside the environment to force the robot to lower itself, showing the capability to also execute vertical movements without compromising the performance. Besides, some blocks have been added to reproduce the terrain's irregularities. With reference to Fig. 2, the heights of the blocks are 0.015 m for the blue, 0.035 m for the green, and 0.02 m for the

red one. The friction coefficients are set to 0.4, 0.6, and 0.8, respectively. The ground friction coefficient value is 1. The observer developed in [33] was also used. The height chosen for the initial configuration of the robot is 0.45 m, while the height of the object's position is 0.80 m. The stance phase has been chosen to last 0.15 s, while the swing phase lasts 0.115 s. The desired trajectory chosen for the object position is a sequence of cubic splines having the initial point at $p_i = [0, -0.7, 0.8]$ m and the final one at $p_f = [0, -4.1, 0.8]$ m.

In all the performed simulations the controller was always successful in preventing the object from sliding and dropping. Code is also available[1].

B. Analysis of the results

The three above-mentioned factors were considered to evaluate the performance of the proposed controller. A two-factor factorial design of the simulations was used to check the significance of factors on the control performance and to determine their optimal levels. Three metrics were considered to evaluate the control performances, namely, (i) the average robustness measure $\mathcal{R}$, evaluated as [15] $\mathcal{R} = T^{-1} \int_0^T 1/\mathcal{H}(t)\,dt$, where the function $\mathcal{H}(\alpha) = \sum_{i=1}^{n_c} \mathcal{H}_i(\alpha_i) = \lambda^{-1} \sum_{i=1}^{n_c} \frac{1}{(\theta_i - \alpha_i)(\alpha_i + \theta_i)}$, is a measure related to how far the friction forces are from the friction cone boundaries, where $\theta_i = \arctan\mu$ is the semiaperture angle of the $i-$th friction cone and $\alpha_i = \arccos \hat{z}_i^{\mathrm{T}} f_{c_i}/||f_{c_i}||$ is the angle between the i.th contact normal $\hat{z}_i$ and the i-th contact force, it was chosen $\lambda = 4$; (ii) the average tracking error $\mathcal{T}$, evaluated as the norm of the linear object displacement from the initially planned trajectory $\mathcal{T} = T^{-1} \int_0^T ||p_{b,ref}(t) - p_b(t)||\,dt$, where $p_{b,ref}$ is the desired position for the object (given by the trajectory) and p_b is its actual position; (iii) the average smoothness $\mathcal{S}$, evaluated as $\mathcal{S} = \frac{T}{\int_0^T ||\dot{\mathcal{V}}_b(t)||\,dt}$. The analysis of the results is carried out leveraging a two-way ANOVA using a significance level $a = 0.05$. All the metrics passed the one-sample Kolmogorov-Smirnov test. Figure 3 shows the mean and the standard deviation of the three considered metrics versus the three factors levels. For the average robustness measure $\mathcal{R}$ (shown in the upper row of Fig. 3), the trends show that it increases when μ increases, while it decreases when either m or d increase. These trends are intuitively explainable: a larger μ is associated with more significant friction cone boundaries, a larger m is associated with larger inertial forces to be counteracted, while a larger d is associated with contact points farther apart. The two-way ANOVA revealed a statistically significantly difference in the metric for different levels of all the considered factors (main effects). The corresponding F- and p-values are: $F = 20.01$, $p < 0.001$ for m, $F = 33329.2$, $p < 0.001$ for μ, $F = 37.26$, $p < 0.001$ for d. A statistically significant change in the metric is also observed for the two-way interaction between the factors μ and d, $F = 11.11$, $p = 0.0024$. The main effects shown earlier can be difficult to interpret when the model includes interactions.

---

[1]https://github.com/prisma-lab/legged-nonprehensile-manip
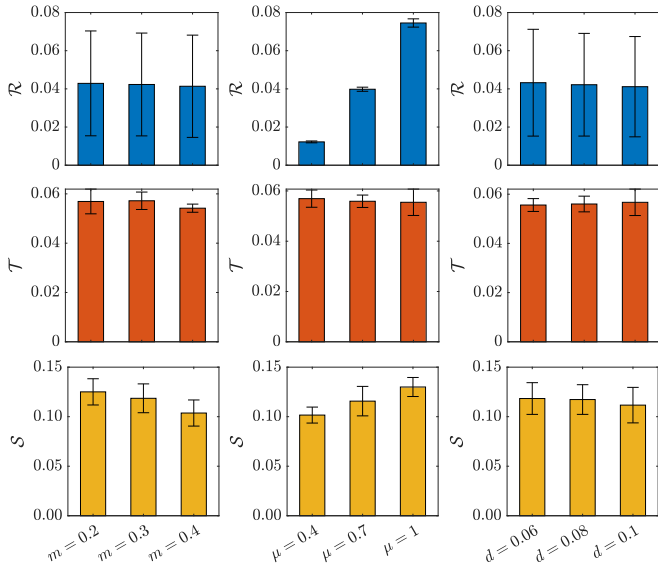
Fig. 3. Performance evaluation results: mean and standard deviation of the robustness $\mathcal{R}$ (upper row), tracking error $\mathcal{T}$ (middle row), and smoothness measure $\mathcal{S}$ (bottom row).
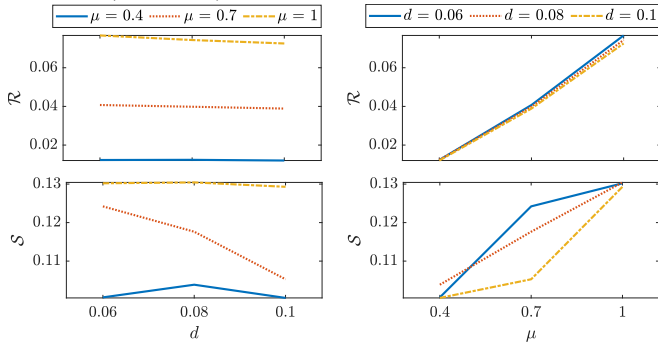

Fig. 4. Performance evaluation results: interaction plots between the factors d and μ for the robustness $\mathcal{R}$ and the smoothness $\mathcal{S}$ measures.

Pairwise comparisons were run to evaluate the simple main effects of μ and d on $\mathcal{R}$. Interaction plots in the upper row of Fig. 4 show an ordinal interaction. The evaluation revealed that, for d, statistically significant differences in $\mathcal{R}$ are observable only between $d = 0.06$ and $d = 0.08$ ($d = 0.1$) with an estimated marginal means difference of 0.0024, $p = 0.0173$ (0.0041, $p < 0.001$). Thus, it can be concluded that the effect of d is most of the time negligible for changes in μ. For the average tracking error $\mathcal{T}$ (shown in the middle row of Fig. 3), no clear trends can be visually identified. Accordingly, the two-way ANOVA revealed no statistically significant changes in the metric for different levels of the considered factors. This effect is expected since, in our settings, object sliding was always successfully prevented. For the smoothness measure $\mathcal{S}$ (shown in the bottom row of Fig. 3), trends are similar to those of the robustness $\mathcal{R}$, i.e., $\mathcal{S}$ increases when μ increases. At the same time, it decreases when either m or d increases. The two-way ANOVA revealed a statistically significant change in the metric when all the considered factors varied. The corresponding F- and p-values are: $F = 60.25$, $p < 0.001$ for m, $F = 100.94$, $p < 0.001$ for μ, $F = 6.47$, $p = 0.023$ for d. Likewise, a statistically significant change in the metric

is also observed for the two-way interaction between the factors μ and d, $F = 4.85$, $p < 0.028$. Pairwise comparisons were run to evaluate the simple main effects of μ and d on $\mathcal{S}$. Interaction plots in the bottom row of Fig. 4 show a ordinal interaction for d (bottom left) and a disordinal interaction for μ (bottom right). The evaluation revealed that, for $d = 0.06$, statistically significant differences in $\mathcal{S}$ are observable only between $\mu = 0.4$ and $\mu = 0.7$ ($\mu = 1.0$) with estimated marginal means differences of -0.0236 (-0.0296) and $p = 0.0048$ ($p = 0.001$). For $d = 0.08$ statistically significant differences in $\mathcal{S}$ are observable between $\mu = 0.4$ and $\mu = 1.0$ with estimated marginal means differences of -0.0266 and $p = 0.002$ while for $d = 0.1$ statistically significant differences in $\mathcal{S}$ are observable between $\mu = 0.4$ ($\mu = 0.7$) and $\mu = 1.0$ with estimated marginal means differences of -0.0289 (-0.024) and $p = 0.001$ ($p = 0.004$). Moreover, when $\mu = 0.7$ statistically significant differences are observable between $d = 0.06$ and $d = 0.1$ with estimated marginal means differences of 0.0189, $p = 0.021$; while for $\mu = 0.4, \mu = 1$ no statistically significant differences are observable. Hence, even in this case, the effect of d is most of the time negligible apart for particular values of μ.

VI. Conclusion and Discussion

A whole-body controller for the nonprehensile transportation of an object through a legged manipulator was presented in this paper. The architecture demonstrated noteworthy performance in simulations performed under different conditions. The framework was tested with varying mass, friction, and dimensions of the transported object on unknown ground. Besides demonstrating the successful accomplishment of the task, the performance was evaluated considering robustness, tracking error, and smoothness metrics.

To summarize, none of the considered factors significantly affect the tracking measure $\mathcal{T}$. This can be attributed to the particular choice of the factor levels and the robot motion parameters. Tracking may be affected when considering a more significant variation of the factors. This will be investigated in future works. Also, it was shown that having a larger μ is always beneficial since it increases robustness and smoothness but the value of the object dimension influences this increment. In real scenarios, this result may be used to design tray-like end-effectors with optimized friction coefficients for such tasks accounting for the transported object dimensions. Moreover, it was shown that heavier objects are generally more challenging to be safely carried. This is reflected in the lower robustness and smoothness measures. In this case, optimal trajectory planning and model-based control methods (e.g., variable orientation [15]) may be employed.

Overall, although the effect of the object dimensions d is negligible, there are cases in which it leads to significant changes. The decrease in robustness and smoothness values when d increases is generally harder to explain. In our view, the choice of the contact model (discrete contact points located at object vertices) may directly affect this result. In the future, we aim to investigate this point further with different contact models and refined approximations.

References

[1] R. de Kervenoael, R. Hasan, A. Schwob, and E. Goh, "Leveraging human-robot interaction in hospitality services: Incorporating the role of perceived value, empathy, and information sharing into visitors' intentions to use social robots," *Tour. Manag*, vol. 78, p. 104042, 2020.

[2] J. Bowen and C. Morosan, "Beware hospitality industry: the robots are coming," *Worldw. Hosp. Tour. Themes*, 2018.

[3] A. H. Basori, "Naocared: Intelligent and communally humanoid assistive robot for elderly care support," *Int. J. Comput. Sci. Netw.*, vol. 20, no. 4, pp. 113–120, 2020.

[4] T. Asafa, T. Afonja, E. Olaniyan, and H. Alade, "Development of a vacuum cleaner robot," *Alex. Eng. J.*, vol. 57, no. 4, pp. 2911–2920, 2018.

[5] P. T. A. Junior, B. d. F. V. Perez, R. Meneghetti, F. d. A. M. Pimentel, and G. N. Marostica, "Hera: Home environment robot assistant," in *II BRAHUR and III Brazilian Workshop on Service Robotics*, 2019.

[6] T. Yamamoto, K. Terada, A. Ochiai, F. Saito, Y. Asahara, and K. Murase, "Development of human support robot as the research platform of a domestic mobile manipulator," *ROBOMECH J.*, vol. 6, no. 1, pp. 1–15, 2019.

[7] S. Chitta, B. Cohen, and M. Likhachev, "Planning for autonomous door opening with a mobile manipulator," in *Proc. IEEE Int. Conf. Rob. Autom.*, 2010, pp. 1799–1806.

[8] J. Garcia-Haro, S. Martinez, and C. Balaguer, "Balance computation of objects transported on a tray by a humanoid robot based on 3D dynamic slopes," in *Proc. IEEE-RAS Int. Conf. Human. Rob.*, 2018, pp. 704–709.

[9] P. Fankhauser and M. Hutter, "Anymal: a unique quadruped robot conquering harsh environments," *Research Features*, no. 126, pp. 54–57, 2018.

[10] C. D. Bellicoso, K. Krämer, M. Stäuble, D. Sako, F. Jenelten, M. Bjelonic, and M. Hutter, "Alma-articulated locomotion and manipulation for a torque-controllable robot," in *Proc. IEEE Int. Conf. Robot. Autom.*, 2019, pp. 8477–8483.

[11] J.-P. Sleiman, F. Farshidian, M. V. Minniti, and M. Hutter, "A unified mpc framework for whole-body dynamic locomotion and manipulation," *IEEE Robot. Autom. Lett.*, vol. 6, no. 3, pp. 4688–4695, 2021.

[12] W. J. Wolfslag, C. McGreavy, G. Xin, C. Tiseo, S. Vijayakumar, and Z. Li, "Optimisation of body-ground contact for augmenting the whole-body loco-manipulation of quadruped robots," in *2020 IEEE/RSJ International Conference on Intelligent Robots and Systems (IROS)*. IEEE, 2020, pp. 3694–3701.

[13] F. Shi, T. Homberger, J. Lee, T. Miki, M. Zhao, F. Farshidian, K. Okada, M. Inaba, and M. Hutter, "Circus anymal: A quadruped learning dexterous manipulation with its limbs," in *2021 IEEE International Conference on Robotics and Automation (ICRA)*. IEEE, 2021, pp. 2316–2323.

[14] F. Ruggiero, V. Lippiello, and B. Siciliano, "Nonprehensile dynamic manipulation: A survey," *IEEE Robot. Autom. Lett.*, vol. 3, no. 3, pp. 1711–1718, July 2018.

[15] M. Selvaggio, J. Cacace, C. Pacchierotti, F. Ruggiero, and P. Robuffo Giordano, "A shared-control teleoperation architecture for nonprehensile object transportation," *IEEE Trans. Robot.*, vol. 38, no. 1, pp. 569–583, 2022.

[16] N. Dini and V. J. Majd, "An mpc-based two-dimensional push recovery of a quadruped robot in trotting gait using its reduced virtual model," *Mech. Mach. Theory*, vol. 146, p. 103737, 2020.

[17] C. D. Bellicoso, C. Gehring, J. Hwangbo, P. Fankhauser, and M. Hutter, "Perception-less terrain adaptation through whole body control and hierarchical optimization," in *Proc. IEEE-RAS 16th Int. Conf. Human. Rob.*, 2016, pp. 558–564.

[18] C. D. Bellicoso, F. Jenelten, P. Fankhauser, C. Gehring, J. Hwangbo, and M. Hutter, "Dynamic locomotion and whole-body control for quadrupedal robots," in *Proc. IEEE/RSJ Int. Conf. on Intell. Rob. Syst.*, 2017, pp. 3359–3365.

[19] C. D. Bellicoso, F. Jenelten, C. Gehring, and M. Hutter, "Dynamic locomotion through online nonlinear motion optimization for quadrupedal robots," *IEEE Robot. Autom. Letters*, vol. 3, no. 3, pp. 2261–2268, 2018.

[20] B. U. Rehman, M. Focchi, J. Lee, H. Dallali, D. G. Caldwell, and C. Semini, "Towards a multi-legged mobile manipulator," in *Proc. IEEE Int. Conf. Robot. Autom.*, 2016, pp. 3618–3624.

[21] M. Risiglione, J.-P. Sleiman, M. V. Minniti, B. Cizmeci, D. Dresscher, and M. Hutter, "Passivity-based control for haptic teleoperation of a legged manipulator in presence of time-delays," in *Proc. IEEE/RSJ Int. Conf. Intell. Rob. Syst.*, 2021.

[22] M. T. Mason and K. M. Lynch, "Dynamic manipulation," in *Proc. IEEE/RSJ Int. Conf. Intell. Robots Syst.*, vol. 1, 1993, pp. 152–159.

[23] K. M. Lynch and T. D. Murphey, "Control of nonprehensile manipulation," in *Control Problems in Robotics*, ser. Springer Tracts in Advanced Robotics, A. Bicchi, D. Prattichizzo, and H. Christensen, Eds. Springer Berlin Heidelberg, 2003, vol. 4, pp. 39–57.

[24] A. Satici, F. Ruggiero, V. Lippiello, and B. Siciliano, "Coordinate-free framework for robotic pizza tossing and catching," in *Proc. IEEE Int. Conf. Robot. Autom.*, 2016, pp. 3932–3939.

[25] M. M. Schill, F. Gruber, and M. Buss, "Quasi-direct nonprehensile catching with uncertain object states," in *Proc. IEEE Int. Conf. Robot. Autom.*, 2015, pp. 2468–2474.

[26] C. Liu, Y. Hayakawa, and A. Nakashima, "Racket control and its experiments for robot playing table tennis," in *Proc. IEEE Int. Conf. Robot. Biomim.*, 2012, pp. 241–246.

[27] F. Bertoncelli, F. Ruggiero, and L. Sabattini, "Linear time-varying MPC for nonprehensile object manipulation with a nonholonomic mobile robot," in *Proc. IEEE Int. Conf. Robot. Autom.*, 2020, pp. 11 032–11 038.

[28] D. Serra, F. Ruggiero, A. Donaire, L. Buonocore, V. Lippiello, and B. Siciliano, "Control of nonprehensile planar rolling manipulation: A passivity-based approach," *IEEE Trans. Robot.*, vol. 35, no. 2, pp. 317–329, 2019.

[29] P. Lertkultanon and Q.-C. Pham, "Dynamic non-prehensile object transportation," in *Proc. Int. Conf. Control Autom. Robot. Vis.*, 2014, pp. 1392–1397.

[30] J. Solanes, L. Gracia, P. Muñoz Benavent, J. Miro, M. Carmichael, and J. Tornero, "Human-robot collaboration for safe object transportaion using force feedback," *Rob. Auton. Syst.*, vol. 107, pp. 196–208, 2018.

[31] R. M. Murray, S. S. Sastry, and L. Zexiang, *A Mathematical Introduction to Robotic Manipulation*, 1st ed. USA: CRC Press, Inc., 1994.

[32] C. Ott, M. A. Roa, and G. Hirzinger, "Posture and balance control for biped robots based on contact force optimization," in *Proc. 11th IEEE-RAS Int. Conf. Humanoid Robots*, 2011, pp. 26–33.

[33] V. Morlando, A. Teimoorzadeh, and F. Ruggiero, "Whole-body control with disturbance rejection through a momentum-based observer for quadruped robots," *Mech. Mach. Theory*, vol. 164, p. 104412, 2021.

[34] M. Bloesch, H. Sommer, T. Laidlow, M. Burri, G. Nuetzi, P. Fankhauser, D. Bellicoso, C. Gehring, S. Leutenegger, M. Hutter *et al.*, "A primer on the differential calculus of 3d orientations," *arXiv preprint arXiv:1606.05285*, 2016.

[35] B. U. Rehman, M. Focchi, M. Frigerio, J. Goldsmith, D. G. Caldwell, and C. Semini, "Design of a hydraulically actuated arm for a quadruped robot," in *Assistive Robotics*. World Scientific, 2015, pp. 283–290.